AIAA Meeting Papers on Disc, January 1996
A9618480, AIAA Paper 96-0519

A linear eddy model for steady-state turbulent combustion

Graham M. Goldin
Georgia Inst. of Technology, Atlanta

Suresh Menon
Georgia Inst. of Technology, Atlanta

AIAA 34th Aerospace Sciences Meeting and Exhibit, Reno, NV Jan 15-18, 1996

A new application of the linear eddy model to steady-state turbulent combustion is presented. The model constructs the single point joint scalar pdf from LEM simulations of scalar decay in homogeneous turbulence. The physical mechanisms of convection by all turbulent scales and molecular diffusion are taken into account, allowing for the inclusion of differential diffusion and extinction affects. By integrating the pdf, mean scalar quantities, in particular the mean chemical reaction rate, are tabulated once and for all as a function of the lower moments. Model pdfs are compared with conventional pdfs using a two variable chemical mechanism. The model is then applied to a turbulent jet flame and the predictions are compared with nonequilibrium experimental results. (Author)

AIAA-96-0519

A LINEAR EDDY MODEL FOR STEADY-STATE TURBULENT COMBUSTION

Graham M. Goldin*
Suresh Menon**

School of Aerospace Engineering
Georgia Institute of Technology

Abstract
A new application of the Linear Eddy Model to steady-state turbulent combustion is presented. The model constructs the single point joint scalar pdf from LEM simulations of scalar decay in homogeneous turbulence. The physical mechanisms of convection by all turbulent scales and molecular diffusion are taken into account, allowing for the inclusion of differential diffusion and extinction affects. By integrating the pdf, mean scalar quantities, in particular the mean chemical reaction rate, are tabulated once and for all as a function of the lower moments. Model pdfs are compared with conventional pdfs using a two variable chemical mechanism. The model is then applied to a turbulent jet flame and the predictions are compared with non-equilibrium experimental results.

1. Introduction

The two prominent approaches to solve the steady-state Navier-Stokes (NS) equations for turbulent reacting flows are the probability density function (pdf) evolution equation method[1] and the moment equation method. The latter include the classical Reynolds averaged NS (RANS)[2], as well as the recently proposed conditioned averages[3]. All these methods require closure, and their success is determined by the accuracy of the models they employ.

In the RANS method, the unclosed higher moments are usually modeled as functions of the available information, namely the solved lower order moments. These unclosed terms can be broadly divided into two groups; one comprising of velocity correlations, such as the Reynolds stress tensor, and the other comprising of scalar averages, such as the mean reaction rate. The velocity correlation fluxes are invariably modeled by mean gradient diffusion, and the present consensus is that despite the known limitations of gradient diffusion, the major source of error lies in the estimate for the scalar averages, especially the mean reaction rate[4,2].

Existing models for the scalar averages assume the statistical distribution of the scalar field (which is specified by the single point joint scalar pdf) using simple analytical functions without taking into account the underlying unsteady turbulent dynamics and molecular mixing. These models include the assumed shape pdf[5] and the Laminar Flamelet model[6], which may employ Beta[7,8] and (clipped) Gaussian[5] functions. Assumed shape methods have obtained successful prediction of flows in chemical equilibrium[5] and flows with moderate departure from equilibrium[8] for simple geometries. However, since the influence of all turbulence scales, as well as molecular diffusion, is implicitly assumed in the pdf, Reynolds (*Re*) and Schmidt (*Sc*) number effects cannot be discerned, and more complex phenomena such as extinction and differential molecular diffusion are precluded due to the difficulty of prescribing the pdf. In addition, owing to the highly non-linear instantaneous reaction rate term, the mean reaction rate is sensitive to the pdf shape, so that large errors in the finite-rate-kinetics flow solution may accrue from small errors in the pdf. This work proposes a new model for the scalar pdf as a function of the lower order moments. Direct account of the unsteady physical processes of turbulent transport and molecular diffusion is taken, overcoming the aforementioned limitations. Although the model formulation is general, it is applied in this paper to non-premixed combustion.

The scalar pdf is constructed from simulations of the Linear Eddy Model (LEM)[9,10]. One of the key features of the LEM, in contrast to most other models such as gradient diffusion, is that *all* turbulence scales are resolved so that the distinct processes of turbulent advection and diffusion-reaction at the smallest scales are captured. This distinction is critical since chemical reaction proceeds at the molecular level when reactants diffuse into contact, and the rate of diffusion (hence chemical conversion for fast chemistry), is strongly affected by the scalar gradients induced by the small scale turbulent motion. The central LEM assumption is that the evolution of the scalar field at the small scales can be adequately captured by a simplified statistical description in one spatial dimension. A 1D formulation allows tractable simulations at high *Re* and *Sc*, a capability impossible in Direct Numerical Simulation (DNS).

Previous applications of the LEM include isothermal mixing in spatially developing turbulent mixing layers[11], plumes[9] and jets[12], and reacting jets with reduced[13] and detailed[14] chemical kinetics. The predicted *Re* and *Sc* dependencies are in accord with turbulence scaling laws and experimental data. In a further application, which has particular significance in this work, the LEM temporal simulation of isothermal scalar decay in homogeneous turbulence obtained quantitative agreement with DNS[15]. Although the diverse range of flow geometries is achieved by altering the initial and boundary conditions, the fundamental LEM kinematic structure is unchanged in all cases, lending credence to its formulation as an accurate and universal mixing model.

2. Model formulation

Since a detailed derivation of the LEM is available in the literature[9,10], only a brief overview is presented in section 2.1. The crux of this work, which is a formulation of the LEM to the

* Graduate Research Assistant, Student Member AIAA.
** Associate Professor, Senior Member AIAA

steady-state moment equation method, is introduced in section 2.2 for general chemistry. Section 2.3 is an application of the model to a reduced chemical mechanism. Henceforth, conventional averaging is denoted by flat overbars, and Favre (density weighted) averaging is denoted by tilde overbars.

2.1 The Linear Eddy Model

The LEM is a spatio-temporal simulation of the evolution of a scalar field in 1D, with turbulent advection treated distinctly from molecular diffusion and reaction, down to the smallest turbulent time and length scales. Since all scales are resolved, the 1D Fickian species equation

$$\frac{\partial Y_k}{\partial t} = \frac{1}{\rho}\frac{\partial}{\partial x}\left(\rho D_k \frac{\partial Y_k}{\partial x}\right) + \dot{w}_k, \qquad (1)$$

is solved without averaging and subsequent modeling. In implementation, equation (1) is solved numerically by central differences on a domain discretized into scalar elements of equal size, δ. Typically six LEM elements are required to resolve the smaller of the Batchelor and Kolmogorov length scales so that sub-element fluctuations are absent and the simulation is grid independent.

The ingenious aspect of the LEM is the mechanism of advection by turbulent eddies, which is modeled in 1D as a stochastic re-arrangement of a portion of the scalar elements along the line. The re-arrangement template is termed the *triplet map*, and is illustrated in figure 1 for an initial linear scalar field on the discrete LEM domain. Triplet mapping does not change the element concentration, consistent with the picture that eddies transport fluid elements and the element concentration can only change by diffusion with neighboring elements. The scalar gradient is however increased, analogous to the effect of a similar sized microscale turbulent eddy on a physical scalar field. Triplet mapping, while not a unique re-arrangement template, has captured most of the principal spectral scaling regimes[10].

The LEM mappings have three stochastic parts. First, the size of an eddy (denoted l in figure 1) is sampled randomly from an eddy-size pdf, denoted $f(l)$. Second, the location center of the mappings are chosen randomly, constrained by the LEM boundary conditions. Third, the mappings are implemented as a Poisson process in time with mean rate parameter λ. The eddy size pdf $f(l)$, as well as the Poisson rate parameter λ, are derived by equating the turbulent diffusivity of the LEM re-arrangements to Kolmogorov cascade diffusivity laws of a scalar in a high Re flow. The resulting governing equations are

$$f(l) = \frac{5}{3}\frac{l^{-8/3}}{\eta^{-5/3} - L^{-5/3}} \qquad \eta \le l \le L \qquad (2)$$

$$\lambda = \frac{54}{5}\frac{\nu Re_t}{L^3}\frac{(L/\eta)^{5/3} - 1}{1 - (\eta/L)^{4/3}} \qquad (3)$$

$$Re_t = \frac{u' L}{\nu} = \left(\frac{L}{\eta}\right)^{4/3}, \qquad (4)$$

where L, η, Re_t and ν are the model integral and Kolmogorov length scales, turbulent Reynolds number and kinematic viscosity respectively. Velocity does not appear explicitly in the LEM, and the turbulence field must be specified *a priori* by providing L and Re_t.

A LEM simulation, on a discrete initial scalar field, progresses as follows. The species equation is continuously advanced at a time step sufficiently small for solution independence. This smoothing process is interrupted by instantaneous triplet mapping events which occur stochastically at a mean Poisson frequency $E = \int \lambda \, dx$. The mapping size l, bound between the limits L and η, is sampled from the pdf $f(l)$ and centered at a random location with probability λ / E. Like all Monte-Carlo methods, the LEM statistics must be averaged over a large ensemble of simulations to wash out stochastic error.

The affect of LEM heat release, which is assumed to occur at constant pressure, is twofold. The first is a change in the viscosity and diffusivity transport co-efficients with the temperature increase. The second is due to the corresponding density decrease which conserves mass by volume expansion. Volume expansion, in turn, causes a decreased vorticity by conserving angular momentum[16]. This reduction in the turbulence is modeled on the linear domain as follows. The kinematic viscosity ν is calculated as a volume average over the scalar field, and η is adjusted from equation (4) by holding the fluctuation velocity u' and integral length scale L constant. The net effect is an increase in η and a decrease in the mapping frequency as heat is released. Since different LEM elements expand to different sizes, while triplet mapping requires equal sized elements, the scalar domain is re-gridded after heat release at the new required resolution, as depicted in figure 2. The overlapping scalar field in each LEM element after re-gridding is mixed without reaction. Note that this spurious mixing is inconsequential since it occurs below the Batchelor length scale where scalar fluctuations are rapidly smoothed.

To illustrate the effect of heat release on product formation, the evolution of the product mass fraction Y_p of a binary mixture in a homogeneous turbulent field is presented in figure 3. The LEM geometry, described in section 2.2, has $L = 2\pi$ and $Re_t = 90$, identical to the simulation of McMurtry et. al.[15]. The reactants have constant transport co-efficients and infinite rate irreversible chemistry with an adiabatic temperature rise of twice the reactant initial temperature. Heat release is seen to decrease the rate of product formation[16].

2.2 The LEM for steady-state turbulent combustion

Before presenting the new model, it is expedient to restate the objective. The moment equation approach requires calculation of mean scalar quantities, such as the mean reaction rate $\overline{\dot{w}_k} = \overline{\dot{w}_k(\rho, T, Y_k)}$, from the solved lower moments, such as the means $\overline{\rho}$, $\tilde{T}$, $\tilde{Y}_k$ and Re_t (ρ, T and Y_k are the fluid density, temperature and k'th species mass fraction, respectively). This is conventionally modeled by assuming a pdf shape $P(\rho, T, Y_k)$, and integrating over all states as

$$\overline{\dot{w}_k} = \int_0^\infty \int_0^\infty \int_0^\infty \int_0^1 \cdots \int_0^1 \dot{w}_k(\rho, T, Y_k) P(\rho, T, Y_k) \, dY_1 \cdots dY_N \, dT \, d\rho. \qquad (5)$$

The objective is to calculate a most likely form of this pdf, satisfying the given lower moments, as opposed to assuming it.

Note that the single point joint scalar pdf can be constructed from the scalar time trace at the point in question.

The LEM is configured to the geometry of a decaying scalar in a stationary homogeneous turbulent field, as in the study by McMurtry et. al.[15]. This entails a periodic domain, with uniform spatial probability of a mapping event. The domain size is set equal to the integral scale L, and mapping epochs occur at a fixed frequency $E = \lambda L$. The initial LEM scalar distribution is assigned, for non-premixed combustion, as the complete segregation of fuel and oxidizer as illustrated in figure 4(a), corresponding to a binary mixture at the maximum variance. For clarity, a single scalar, viz. the mixture fraction f, is shown, although the method is readily extended to multiple species with different molecular diffusivities.

Under the action of molecular diffusion and turbulent stirring (mapping events), the scalar variance $g = (f - \tilde{f})^2$ decays toward zero. Figure 4(b) is a plot of the spatial distribution of f at some later time. The central concept of this work is to approximate the actual scalar time trace at a point in a turbulent flow by the scalar distribution in a LEM simulation. The LEM spatial axis (the x/L axis in figure 3) is transformed to a time axis which may be interpreted as a Taylor hypothesis (also referred to as a frozen turbulence approximation), and holds exactly for isotropic turbulence. From this time trace the single point joint scalar pdf can be constructed by binning over all states.

The implementation in a RANS solver is as follows. During the solution of the modeled transport equations for the lower moments (see section 3 below), assume that the numerical values $\overline{\rho}$, $\tilde{T}$, $\tilde{Y}_k$ and Re_t are attained at one point in the flow-field. In the method proposed above, a separate, full-kinetic LEM simulation is conducted with the appropriate initial conditions and turbulent scales, as detailed later, such that the LEM pdf has lower moments $\overline{\rho}^{LEM}$, $\tilde{T}^{LEM}$, $\tilde{Y}_k^{LEM}$ and Re_t^{LEM} that exactly match those in the flow-field (viz. $\overline{\rho}^{LEM} = \overline{\rho}$, $\tilde{T}^{LEM} = \tilde{T}$, $\tilde{Y}_k^{LEM} = \tilde{Y}_k$ and $Re_t^{LEM} = Re_t$). The spatial point in the RANS solution is then assumed to have the LEM pdf and scalar means such as $\overline{\dot{w}}_k$ and $\overline{RT}$ (R is the gas constant) are obtained from equation (5). Although only first moments have been matched in the above example, higher moments and correlations can be equated to increase the accuracy, provided that their modeled RANS transport equations are accurate.

The fact that the LEM simulation is time accurate is of no consequence here since the physical time trace satisfying given higher moments is used, independent of the trace history. Reflecting this, the pdf contains no time information.

As opposed to performing the LEM simulations and pdf integrations during the solution of the RANS, the calculations may be performed once and for all over the entire range of $\overline{\rho} - \tilde{T} - \tilde{Y}_k - Re_t$ space and the scalar means tabulated as

$$\overline{\dot{w}}_k = \overline{\dot{w}}_k \{\overline{\rho}, \tilde{T}; \tilde{Y}_k; \mathrm{Re}_t\}, \qquad (6)$$

where $\overline{\rho}$, $\tilde{T}$, $\tilde{Y}_k$ and Re_t are the table parameters. The curly braces denote a tabular format, and are not to be confused with the approximation of the mean reaction rate by its instantaneous (laminar) expression. During the numerical solution of the RANS equations, the table is searched and interpolated as a function of the solution variables $\overline{\rho}$, $\tilde{T}$, $\tilde{Y}_k$ and Re_t.

Owing to the computational economy of the LEM, tables for complex chemistry at high Re can be affordably assembled. However, for a large number of chemical species, the table size may become intractably large if all mean species $\tilde{Y}_k$ are parametized. As an alternative, the table may be parametized by an appropriate reduced subset of mean species, with some loss in generality.

Sc effects are implicit in the model. For example, two LEM simulations at different Sc that have the same means $\overline{\rho}$, $\tilde{T}$, $\tilde{Y}_k$ and Re_t will have different $\overline{\dot{w}}_k$. Differential diffusion may be incorporated without difficulty into the LEM simulation, and since the full scalar pdf $P(\rho, T, Y_k)$ is constructed, ignition and extinction can be modeled in a RANS solution. These issues will be addressed in a future study. An additional advantage of the model is that, unlike most assumed shape methods, moments higher than first order are not required to specify the pdf. One limitation of the present model is the inability and apparent difficulty in addressing the fluctuating pressure field.

The LEM triplet map, while an excellent model for the small scale motion, is a somewhat crude approximation for the integral scales, and is a poor model for the anisotropic coherent structures. The model is hence incapable of capturing certain large scale features. However, the large scale effect of intermittency can be captured (intermittency occurs when the time trace is located at $f = 0$ or $f = 1$, such as in figure 4(a)). In this work, the integral scale is assumed to be the largest eddy, and is set equal to the jet nozzle diameter d. Although the size of the coherent structures in a turbulent jet increase downstream, and may be thus much larger than d, this is not considered to have an extreme affect because the large scales, governed by the eddy-size pdf $f(l)$, occur infrequently.

Another issue which requires justification is the assumption of an initial binary mixture (see figure 4(a)), as opposed to a plug-flow type initial distribution, which has evenly spaced 'slabs' of fuel and oxidizer. The latter case decays faster due to the increased scalar gradients. McMurtry et. al.[15] performed LEM simulations in an identical geometry for a range of initial scalar distributions, and showed that the field became independent of the initial scalar length scale after a short transient.

2.3 Application to a reduced chemical mechanism

The model is demonstrated using a two-variable (f,n) reduced chemical mechanism for H_2-air combustion[17]. Under the assumptions of unity Lewis number for all species, constant pressure, low Mach number, low bouyancy and adiabaticity, nine species and temperature are completely specified by the conserved mixture fraction f, and a progress variable n. Since the allowable domain in $f - n$ space is tri-angular, the progress variable is normalized as

$$n^* = \frac{n - n_{min}(f)}{n_{max}(f) - n_{min}(f)}, \tag{7}$$

for graphical presentation on a rectangular $f-n$ domain. The limits $f=0$ and $f=1$ correspond to oxidizer and fuel, and at a fixed f, $n^*=0$ and $n^*=1$ indicate the equilibrium and the mixed without reaction limits respectively.

Comparison is made with two conventional models. The first is the assumed shape pdf[8] which requires RANS equations for the first two moments of f (mean $\tilde{f}$ and variance $\tilde{g}$), and the mean reaction progress, $\tilde{n}^*$. The joint pdf of f and n^* is invariably modeled as[8]

$$P(f,n^*) = P_1(f)\,P_2(n^*), \tag{8}$$

with $P_1(f)$ assumed as a Beta function and $P_2(n^*)$ as a Dirac delta function at the mean, viz. $P_2(n^*) = \delta(n^* - \tilde{n}^*)$. It is common[8] to model a n^* variance equation and modify $P_2(n^*)$ by Dirac delta functions at $n^*=0$ and $n^*=1$. Since the LEM pdf does not require the variance of n^*, this pdf form is discarded for fair comparison. The mean species and mean reaction rate $\overline{\dot{w}}_n$, at a point in an assumed shape pdf RANS solution are functions of $\tilde{f}$, $\tilde{g}$ and $\tilde{n}^*$ at the point.

The second conventional method compared is the Laminar Flamelet model[6], which considers a turbulent flame brush as an ensemble of unsteady diffusion flamelets. Each flamelet has the structure of a steady strained laminar diffusion flame (Tsuji flame). The Tsuji flame is characterized by the single parameter $\chi_{f=f_{sto}}$, which is the scalar dissipation, defined as

$$\chi = 2D\frac{\partial f}{\partial x_i}\frac{\partial f}{\partial x_i}, \tag{9}$$

at the point of stochiometric mixture fraction. In a turbulent diffusion flame calculation, the mean species at a point are obtained from the statistical distribution of the flamelet ensemble,

$$\tilde{Y}_k = \int_0^1\int_0^\infty Y_k(f,\chi_{f=f_{sto}})\,P(f,\chi_{f=f_{sto}})\,d\chi\,df. \tag{10}$$

The pdf $P(f,\chi_{f=f_{sto}})$ is commonly assumed uncorrelated as

$$P(f,\chi_{f=f_{sto}}) = P_1(f)\,P_2(\chi), \tag{11}$$

with $P_1(f)$ assumed as a Beta function, and $P_2(\chi)$ as a log-normal distribution with a variance of 2,

$$P_2(\chi) = \frac{1}{\chi\sqrt{4\pi}}\exp\left\{-\frac{1}{4}\left(\ln\frac{\chi}{\tilde{\chi}}+1\right)^2\right\}. \tag{12}$$

The mean scalar dissipation is modeled in the RANS solution as

$$\tilde{\chi} = C_\chi\frac{\tilde{\varepsilon}}{\tilde{k}}\tilde{g}, \tag{13}$$

where $\tilde{k}$ and $\tilde{\varepsilon}$ are the mean turbulent kinetic energy and its dissipation, and the constant $C_\chi = 2$. The mean scalar dissipation, which is a measure of the intensity of local mixing, may be interpreted as a Re_t parameter. For a given flamelet library $Y_k(f,\chi_{f=f_{sto}})$, the mean species at a point in a Laminar Flamelet RANS solution are functions of $\tilde{f}$, $\tilde{g}$, $\tilde{k}$ and $\tilde{\varepsilon}$ at the point.

The above two methods assume the statistical distribution of the fluctuating scalar field (equations (8) and (11)) at a point without accounting for the physical passage of turbulent eddies, or the molecular diffusion properties of the scalar.

The LEM species equation (1), reduced to the (f,n) chemistry is

$$\frac{\partial f}{\partial t} = \frac{1}{\rho}\frac{\partial}{\partial x}\left(\rho D\frac{\partial f}{\partial x}\right) \tag{14}$$

and

$$\frac{\partial n}{\partial t} = \frac{1}{\rho}\frac{\partial}{\partial x}\left(\rho D\frac{\partial n}{\partial x}\right) + \dot{w}_n. \tag{15}$$

The discrete values of f and n in each LEM cell evolve subject to the deterministic equations (14) and (15), and the stochastic stirring events governed by equations (2) through (4).

Results from an arbitrary LEM simulation are shown in figures (4) to (6) for a fuel of 22% Argon (mol) in H_2, which has a stochiometric mixture fraction $f_{sto} = 0.161$. Since f is a conserved scalar, the Favre averaged mixture fraction $\tilde{f}$, remains constant throughout the simulations, and is set equal to f_{sto} here. Figure 4(a) is the initial scalar field, which has maximum variance $\tilde{g} = \tilde{f} - \tilde{f}^2$. Molecular diffusion causes the scalar variance to decay in time as the simulation proceeds. The rate of scalar decay increases with Re_t since the more frequent mapping events amplify the scalar gradients, leading to an increased diffusion rate. In turn, the departure from chemical equilibrium increases as the diffusion time scale approaches the chemical time scale.

For $L = 0.052m$, corresponding to the jet diameter of the experimental geometry[18] chosen, and $Re_t = 60$, the instantaneous scalar field at $\tilde{g} = 0.01$ is plotted in figures 4(b)-(d). These show the spatial distributions of f, n^* and χ respectively, which have spatial means $\tilde{f} = f_{sto}$,, $\tilde{n}^* = 0.0633$ and $\tilde{\chi} = 21.7s^{-1}$. The LEM equivalent of the scalar dissipation (equation (9)) is

$$\chi = 2D\left(\frac{\partial f}{\partial x}\right)^2. \tag{16}$$

By transforming the spatial axis to a time axis, scatter plots (created by placing a probe in the time trace) and pdf plots

(created by binning the time trace) for a *point* in a turbulent diffusion flame with $\widetilde{f} = f_{sto}$, $\widetilde{g} = 0.01$, $\widetilde{n}^* = 0.0633$ and $\widetilde{\chi} = 21.7 s^{-1}$ may be constructed. Figure 5(a) presents a scatter plot of temperature in mixture fraction space using 2500 points from an ensemble of the above described LEM simulations. Figure 5(b) is a corresponding experimental plot[18], and the similarity is evident. Both plots display sub-equilibrium temperatures, with the greatest deviation from equilibrium occuring around stochiometric mixture fraction.

Figure 6 presents LEM pdf plots constructed from an ensemble of 10000 LEM realizations, as well as their corresponding conventional pdf models. Figure 6(a) is the single point joint scalar pdf $P(f,n^*)$ with lower moments $\widetilde{f} = f_{sto}$, $\widetilde{g} = 0.01$ and $\widetilde{n}^* = 0.0633$. Note that the pdf peak has been truncated for clarity. Elements closest to stochiometric mixture ($f_{sto} = 0.161$) are at greater non-equilibrium ($n^* > 0$) than off-stochiometric elements, which is synonymous with the experimental data in figure 5(b). The conventional assumed shape pdf, equation (8), with the same lower moments $\widetilde{f}$, $\widetilde{g}$ and $\widetilde{n}^*$ is plotted in figure 6(b). The model assumes that all fluid elements passing over the point have the same (normalized) departure from equilibrium, which is clearly a big assumption.

Figure 6(c) is a plot of the single point joint scalar pdf $P(f,\chi)$ with lower moments $\widetilde{f} = f_{sto}$, $\widetilde{g} = 0.01$ and $\widetilde{\chi} = 21.7 s^{-1}$, and with the pdf peak truncated at a height of 5. The conventional Laminar Flamelet pdf, equations (11) and (12), with the same lower moments $\widetilde{f}$, $\widetilde{g}$ and $\widetilde{\chi}$ is plotted in figure 6(d). The LEM time trace has large periods with χ near zero, and short bursts of strained diffusion layers with large χ (see figure 4(d)). Recalling that both plots have the same mean scalar dissipation $\widetilde{\chi}$, the LEM trace has greater probability of low χ and concentrated regions of very large χ, with a dependence stronger than log-normal. The LEM pdf does not show significant correlation between f and χ, in agreement with the conventional assumption of f and χ independence. The present approach is valid in the connected reaction (partial premixed) zone where flamelets are no longer distinct laminar flames from $f = 0$ to $f = 1$, and the classical Laminar Flamelet model breaks down. Also, it can be used to predict local extinction without resorting to heuristic Percolation theory[6].

By performing simulations over a range of $\widetilde{f}$ and Re_t (hence $\widetilde{n}$ and $\widetilde{\chi}$), the entire discretized $\widetilde{f} - \widetilde{g} - \widetilde{n}$ and $\widetilde{f} - \widetilde{g} - \widetilde{\chi}$ space can be tabulated. Mean scalars ($\overline{\dot{w}}_n$, $\widetilde{Y}_k$ etc.) are stored in a look-up table as functions of the parameters $\widetilde{f}$ and $\widetilde{g}$, and $\widetilde{n}$ or $\widetilde{\chi}$. The $\widetilde{f} - \widetilde{g} - \widetilde{n}$ table is used in a RANS solver with a transport equation for $\widetilde{n}$, whereas the $\widetilde{f} - \widetilde{g} - \widetilde{\chi}$ table is used in a Laminar Flamelet type application. It is emphasized that for a given chemistry, the LEM table is constructed once and for all. The run-time cost in a RANS solver is equal to the conventional assumed shape approach if the latter is implemented as a look-up table.

In summary, the LEM time trace with lower order means $\{\widetilde{f};\widetilde{g};\widetilde{n}\}$ or $\{\widetilde{f};\widetilde{g};\widetilde{\chi}\}$ is used to calculate required mean scalar quantities in a RANS solver with transport equations for the equivalent means $\{\widetilde{f};\widetilde{g};\widetilde{n}\}$ or $\{\widetilde{f};\widetilde{g};\widetilde{\chi}\}$.

3. Application in a RANS solver

The RANS are closed in this work with a conventional $k-\varepsilon$ turbulence model[19]. The dimensional conservation equations with the (f,n) reduced chemistry are:

$$\frac{\partial \overline{\rho}}{\partial t} + \frac{\partial}{\partial x_i}(\overline{\rho}\widetilde{u}_i) = 0 \tag{17}$$

$$\frac{\partial}{\partial t}(\overline{\rho}\widetilde{u}_i) + \frac{\partial}{\partial x_j}(\overline{\rho}\widetilde{u}_i\widetilde{u}_j) = -\frac{\partial \overline{p}}{\partial x_i} + \frac{\partial}{\partial x_j}\left((\mu+\mu_t)S_{ij} - \tfrac{2}{3}\overline{\rho}\widetilde{k}\delta_{ij}\right) \tag{18}$$

$$\frac{\partial}{\partial t}(\overline{\rho}\widetilde{k}) + \frac{\partial}{\partial x_i}(\overline{\rho}\widetilde{u}_i\widetilde{k}) = \frac{\partial}{\partial x_i}\left((\mu+\mu_t)\frac{\partial \widetilde{k}}{\partial x_i}\right) + P_k - \overline{\rho}\widetilde{\varepsilon} \tag{19}$$

$$\frac{\partial}{\partial t}(\overline{\rho}\widetilde{\varepsilon}) + \frac{\partial}{\partial x_i}(\overline{\rho}\widetilde{u}_i\widetilde{\varepsilon}) = \frac{\partial}{\partial x_i}\left((\mu+\frac{\mu_t}{\sigma_\varepsilon})\frac{\partial \widetilde{\varepsilon}}{\partial x_i}\right) + (C_{\varepsilon 1}P_k - C_{\varepsilon 2}\overline{\rho}\widetilde{\varepsilon})\frac{\widetilde{\varepsilon}}{\widetilde{k}} \tag{20}$$

$$\frac{\partial}{\partial t}(\overline{\rho}\widetilde{f}) + \frac{\partial}{\partial x_i}(\overline{\rho}\widetilde{u}_i\widetilde{f}) = \frac{\partial}{\partial x_i}\left((\frac{\mu}{Sc} + \frac{\mu_t}{Sc_t})\frac{\partial \widetilde{f}}{\partial x_i}\right) \tag{21}$$

$$\frac{\partial}{\partial t}(\overline{\rho}\widetilde{g}) + \frac{\partial}{\partial x_i}(\overline{\rho}\widetilde{u}_i\widetilde{g}) = \frac{\partial}{\partial x_i}\left((\frac{\mu}{Sc} + \frac{\mu_t}{Sc_t})\frac{\partial \widetilde{g}}{\partial x_i}\right) + C_{g1}\mu_t\left(\frac{\partial \widetilde{f}}{\partial x_i}\right)^2 - C_{g2}\overline{\rho}\widetilde{g}\frac{\widetilde{\varepsilon}}{\widetilde{k}} \tag{22}$$

$$\frac{\partial}{\partial t}(\overline{\rho}\widetilde{n}) + \frac{\partial}{\partial x_i}(\overline{\rho}\widetilde{u}_i\widetilde{n}) = \frac{\partial}{\partial x_i}\left((\frac{\mu}{Sc} + \frac{\mu_t}{Sc_t})\frac{\partial \widetilde{n}}{\partial x_i}\right) + \overline{\dot{w}}_n, \tag{23}$$

where

$$S_{ij} = \frac{\partial \widetilde{u}_i}{\partial x_j} + \frac{\partial \widetilde{u}_j}{\partial x_i} - \tfrac{2}{3}\delta_{ij}\frac{\partial \widetilde{u}_k}{\partial x_k} \tag{24}$$

$$\mu_t = C_\mu \overline{\rho}\frac{\widetilde{k}^2}{\widetilde{\varepsilon}} \tag{25}$$

$$P_k = (\mu_t S_{ij} - \tfrac{2}{3}\overline{\rho}\widetilde{k}\delta_{ij})\frac{\partial \widetilde{u}_i}{\partial x_j} \tag{26}$$

$$\overline{p} = \overline{\rho}R\widetilde{T}. \tag{27}$$

The model constants $C_\mu, C_{\varepsilon 1}, C_{\varepsilon 2}, \sigma_\varepsilon, C_{g1}, C_{g2}, Sc$ and Sc_t are 0.09, 1.44, 1.92, 1.3, 2.0, 2.0, 0.7 and 1.0 respectively.

The system of equations (17)-(27) is solved in an axi-symmetric frame using the finite volume method of Jameson et. al.[20]. Inviscid fluxes are calculated with a third order MUSCL-TVD[21] AUSM[22] scheme, and marched to a steady-state with a five-stage Runge-Kutta algorithm[23]. At steady state, the temporal terms on the LHS of equations (17)-(23) approach zero.

Simulations were conducted using both $\widetilde{f} - \widetilde{g} - \widetilde{n}$ and $\widetilde{f} - \widetilde{g} - \widetilde{\chi}$ look-up tables with a size of 50x25x15. Tables were

appropriately clustered around $\tilde{f} = f_{sto}$ and $\tilde{g} = 0$. Both tables contain the scalar means $\tilde{Y}_k$, $\tilde{T}$ and $\tilde{RT}$, while the $\tilde{f} - \tilde{g} - \tilde{n}$ table has the additional quantity $\overline{\dot{w}}_n$ tabulated. During solution of the RANS equations, tri-linear interpolation is used to approximate the mean scalars between table node points.

4. Results and discussion

The NS code validation follows in section 4.1. A comparison of the new theory with experimental data is presented in section 4.2. Section 4.3 presents future model prospects.

4.1 Code validation

The baseline NS solver and $k-\varepsilon$ model were validated for an axi-symmetric isothermal turbulent jet (results not presented here). Although the mean velocity decay rate was over-predicted, in accordance with $k-\varepsilon$ theory[19], perfectly self-similar and grid-independent mean velocity, turbulence intensity and Reynolds stress profiles were attained.

Experimental[24] and predicted mean mixture fraction and temperature radial plots at axial locations $x/d = 23$, 90 and 135 for a turbulent H_2 jet flame are shown in figure 7. Reasonable agreement is obtained, except for the far-field temperature. This is due to an under-estimate of the mean mixture fraction decay (figure 7(c)) and, to some extent, the neglect of flame radiation.

4.2 Application to a non-equilibrium flame

The LEM pdf approach was applied to the experimental H_2 flame of Drake et. al.[25]. Measured OH radical concentration profiles are compared against model predictions using the $\tilde{f} - \tilde{g} - \tilde{n}$ and $\tilde{f} - \tilde{g} - \tilde{\chi}$ approaches in figures 8 and 9 respectively. The open circles are the measured mean OH concentrations, and the plus signs are the hypothetical measured mean OH equilibrium concentrations, calculated from the major species. The solid curve is the LEM predicted mean OH concentration, and the dashed line is the corresponding LEM mean equilibrium OH concentration.

In both cases the near field OH is under-predicted. Since the equilibrium concentrations are reasonably well predicted, this implies either an error in both the non-equilibrium variables $\tilde{n}$ and $\tilde{\chi}$, or a chemistry error due to the reduced mechanism assumptions.

Simulations using the conventional assumed shape β-pdf equation (8) are indicated by the dotted line in figure 8. The conventional results are essentially identical to the LEM pdf, so the superiority of the LEM model is not conclusively demonstrated in this example. Analysis of the LEM and assumed shape $\tilde{f} - \tilde{g} - \tilde{n}$ tables reveals that although their pdfs are considerably different (figures 6(a) and (b)), the pdf means $\tilde{Y}_{OH}\{\tilde{f},\tilde{g},\tilde{n}\}$ and $\overline{\dot{w}}_n\{\tilde{f},\tilde{g},\tilde{n}\}$ are similar.

4.3 Future prospects

The LEM pdf model can be tractably extended to general chemistry for premixed as well as non-premixed steady-state combustion. The joint pdf $P(\rho,T,Y_k)$ can be constructed as a function of its lower moments, allowing ignition and extinction modeling in a RANS solver. Differential diffusion can be included in the LEM simulation and its effect on $P(\rho,T,Y_k)$ studied. These issues are under investigation and will be reported in the near future.

Conclusions

A Linear Eddy Model application to steady-state turbulent combustion has been formulated. The model is based on the assumption that the actual scalar time trace at a point in a turbulent flow can be well approximated by the spatial scalar distribution in a LEM simulation. By matching the lower order moments in a RANS solver with the LEM lower order moments, look-up tables for required scalar means may be constructed.

Although the LEM table is more expensive to construct than conventional pdf tables, the LEM table is calculated only once, and has equal look-up cost in a RANS solver. The model offers potentially increased accuracy at no additional computational expense.

The model has been applied to a RANS solution of a turbulent jet flame using a two variable chemical mechanism. Conclusive superiority over conventional methods has not yet been demonstrated, although the method allows extension to general chemistry with differential diffusion.

References

1. Pope, S.B. (1985) "PDF Methods for Turbulent Reactive Flows", *Prog. Energy Comb. Sci.* **11**, 119
2. Libby, P.A. and Williams, F.A. (1980) "Fundamental Aspects", in *Turbulent Reacting Flows* (Libby, P.A. and Williams, F.A. ed) Springer-Verlag
3. Bilger, R.W. (1992) "Conditional Moment Closure for Turbulent Reacting Flows", *Phys. Fluids A* **5**, 436
4. Bilger, R.W. (1989) "Turbulent Diffusion Flames", *Ann.Rev. Fluid. Mech.* **21**, 101
5. Lockwood, F.C. and Naguib, A.S. (1975) "The Prediction of the Fluctuations in the Properties of Free, Round-jet, Turbulent, Diffusion Flames", *Comb. and Flame* **24**, 109
6. Peters, N. (1984) "Laminar Diffusion Flamelet Models in Non-Premixed Turbulent Combustion", *Prog. Energy Comb. Sci.* **10**, 319
7. Girimaji, S. S. (1991) "Assumed β-pdf Model for Turbulent Mixing: Validation and Extension to Multiple Scalar Mixing", *Comb. Sci. and Tech.* **78**, 177
8. Janicka, J. and Kollmann, W. (1979) "A Two-Variables Formalism for the Treatment of Chemical Reactions in Turbulent H_2-Air Diffusion Flames", *Seventeenth Symp. (Int.) on Comb.*, The Combustion Institute, 421
9. Kerstein, A.R. (1988) "Linear Eddy Model of Turbulent Scalar Transport and Mixing", *Comb. Sci. and Tech.* **60**, *391*
10. Kerstein, A.R. (1991) "Linear Eddy Modeling of Turbulent Transport. Part 6. Microstructure of Diffusive Scalar Mixing Fields", *J. Fluid Mech.* **231**, 361
11. Kerstein, A.R. (1989) "Linear Eddy Modeling of Turbulent Transport II: Application to Shear Layer Mixing", *Comb. and Flame*. **75**, 397
12. Kerstein, A.R. (1990) "Linear Eddy Modeling of Turbulent Transport. Part 3. Mixing and Differential Molecular Diffusion in Round Jets", *J. Fluid Mech.* **216**, 411
13. Kerstein, A.R. (1992) "Linear Eddy Modeling of Turbulent Transport. Part 4. Diffusion-Flame Structure", *Comb. Sci. and Tech.* **81**, 75

14. Calhoon, W.H., Menon, S. and Goldin, G. (1995) "Comparison of Reduced and Full Chemical Mechanisms for Non-Premixed Turbulent Hydrogen-Air Jet Flames", *Comb. Sci. and Tech.* **104**, 115
15. McMurtry, P.A., Gansuage, T.C., Kerstein, A.R. and Krueger, S.K. (1993) "Linear Eddy Simulations of Mixing in a Homogeneous Turbulent Flow", *Phys. Fluids A* **5**, 1023
16. McMurtry, P.A., Riley, J.J. and Metcalfe, R.W (1989) "Effects of heat release on the large-scale structure in turbulent mixing layers", *J. Fluid. Mech.* **199**, 297
17. Chen, J.Y. and Kollman, W. (1990) "Chemical Models for Pdf Modeling of Hydrogen-Air Nonpremixed Turbulent Flames", *Comb. and Flame* **79**, 75
18. Magre, P. and Dibble, R. (1988) "Finite Chemical Kinetic Effects in a Subsonic Hydrogen Flame" *Comb. and Flame* **73**, 195
19. Launder, B.E. and Spalding, D.B. (1974) "The Numerical Computation of Turbulent Flows", *Comp. Meth. in App. Mech. and Eng.* **3**, 269
20. Jameson, A., Schmidt, W. and Turkel, E. (1981) "Numerical Solution of the Euler Equations by Finite Volume Methods Using Runge-Kutta Time Stepping Schemes", *AIAA-81-1259*
21. Anderson, W.K., Thomas, J.L. and Van Leer, B. (1986) "Comparisons of Finite Volume Flux Splittings for the Euler Equations", *AIAA J.* **9**, 1453
22. Liou, M.S. and Steffen, C.J. (1993) "A New Flux Splitting Scheme", *J. Comp. Physics* **107**, 23
23. Martinelli, L. and Jameson, A. (1988) "Validation of a Multigrid Method for the Reynolds Averaged Equations", *AIAA-88-0414*
24. Barlow, R.S. and Carter, C.D. (1994) "Nitric Oxide Formation in Hydrogen Jet Flames", *Comb. and Flame* **97**, 261
25. Drake, M.C., Pitz, R.W., Fenimore, C.P., Lucht, R.P., Sweeney, D.W., and Laurendeau M.M. (1984) "Measurements of Superequilibrium Hydroxyl Concentrations in Turbulent Non-Premixed Flames Using Saturated Fluorescence", *Twentieth Symp. (Int.) on Comb.*, The Combustion Institute, 327

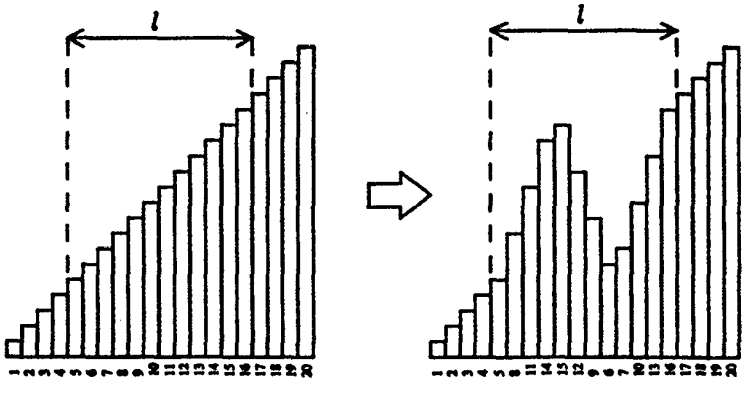

Figure 1:
Schematic illustration of a triplet mapping of an initial uniform scalar gradient. The re-arrangement makes three compressed images of the original segment by taking every third scalar element, then replaces the original segment by the three images with the middle field inverted.

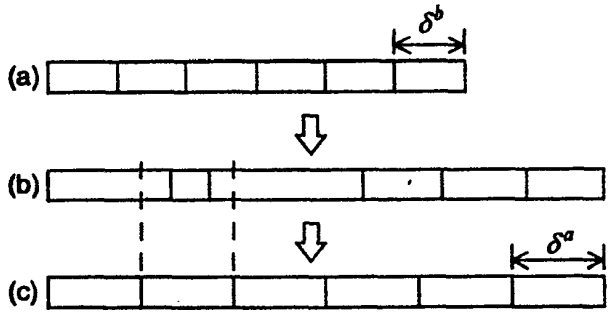

Figure 2:
Schematic illustration of volume expansion and re-gridding.
(a) Original LEM field with element size δ^b before heat release.
(b) LEM field after heat release and volume expansion.
(c) LEM field re-gridded and mixed at new resolution δ^a.

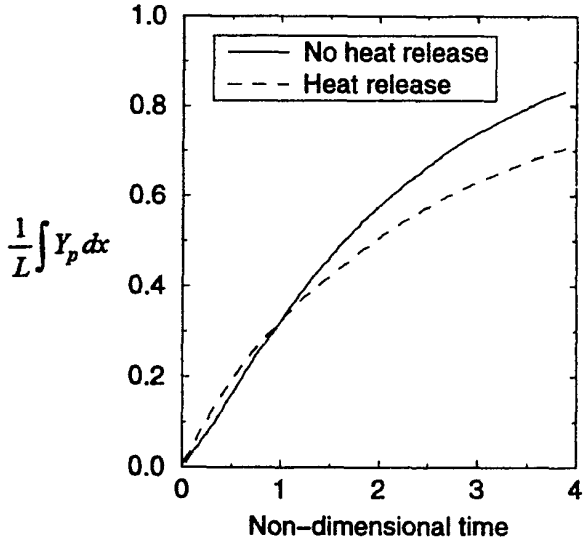

Figure 3: LEM evolution of the total product mass fraction

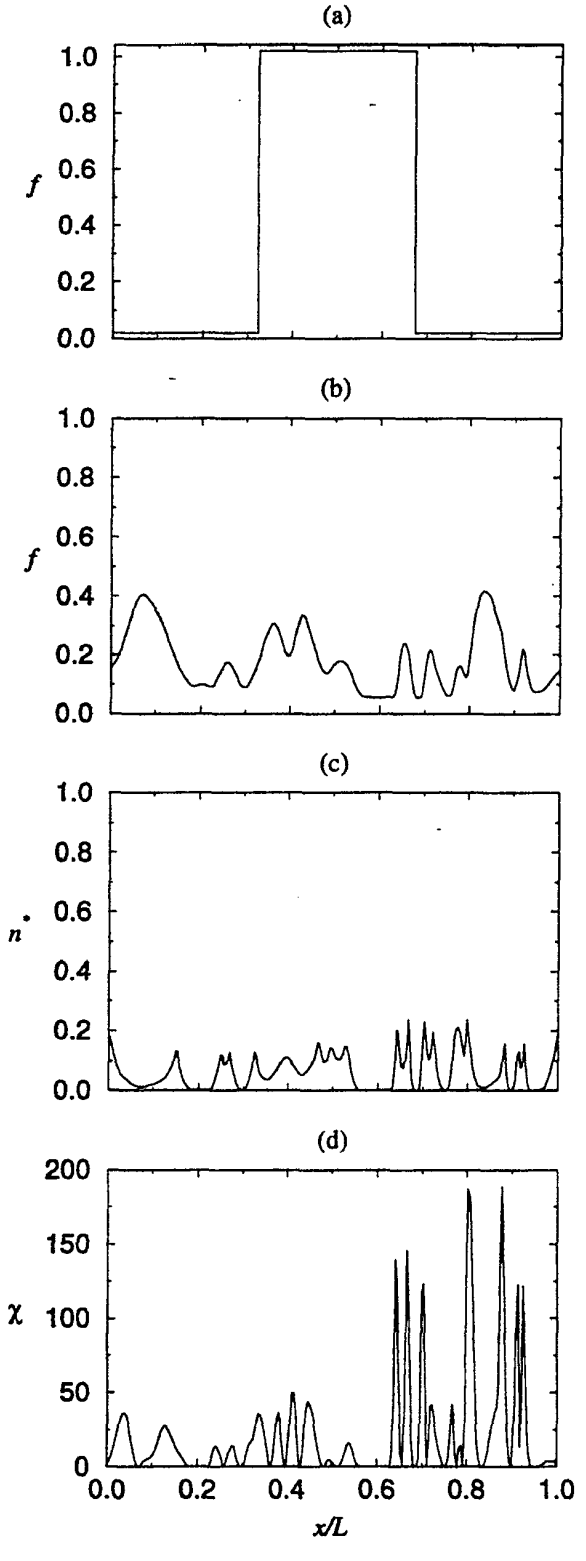

Figure 4: Instantaneous LEM scalar distribution
(a) Initial binary mixture fraction, $\tilde{f} = f_{ini} = 0.161$
(b) Mixture fraction at a later time, $\tilde{f} = f_{ini}, \tilde{g} = 0.01$
(c) Normalized progress variable, $\tilde{f} = f_{ini}, \tilde{g} = 0.01, \tilde{n}^* = 0.0633$
(d) Scalar dissipation, $\tilde{f} = f_{ini}, \tilde{g} = 0.01, \tilde{\chi} = 21.7 s^{-1}$

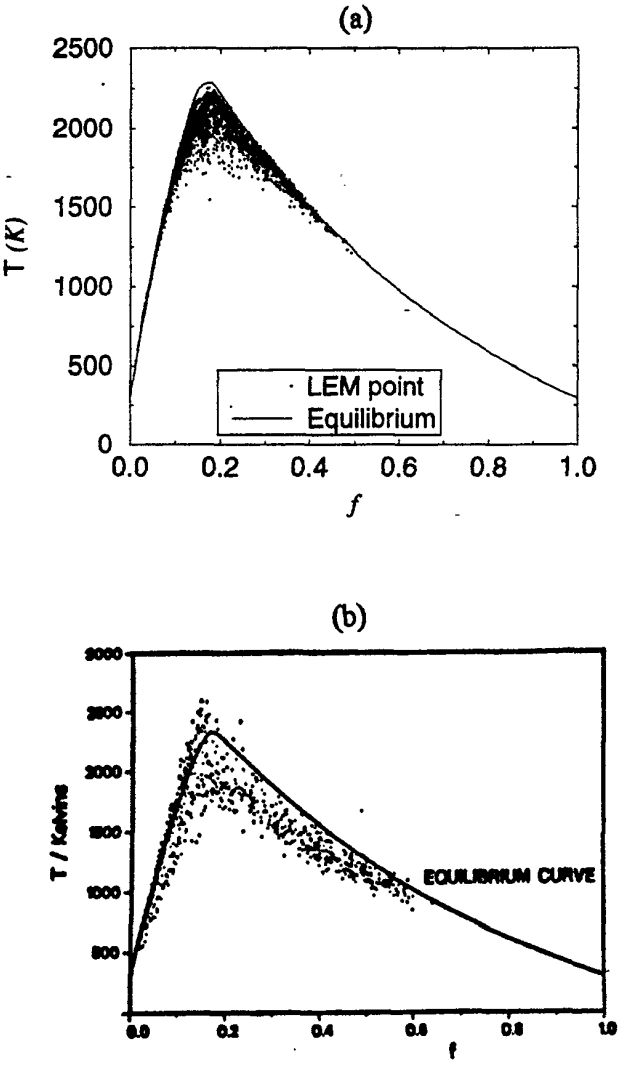

Figure 5: Temperature scatter plots in mixture fraction space
(a) LEM points
(b) Experimental[18]

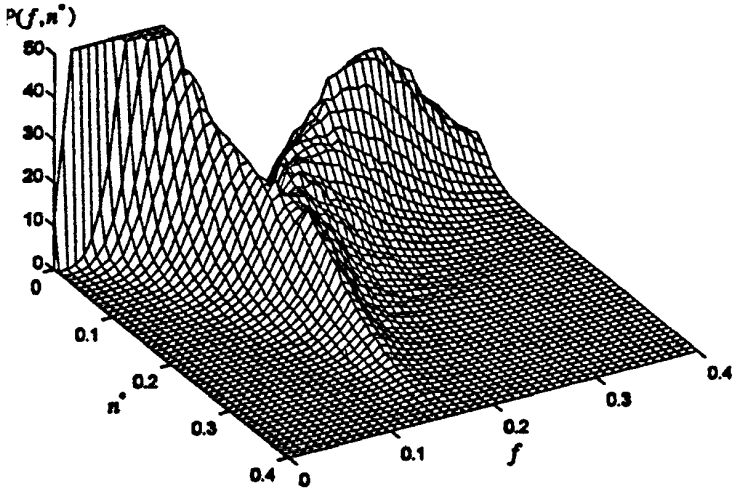

Figure 6(a): LEM pdf $P(f,n^*)$
$\tilde{f} = f_{so}, \tilde{g} = 0.01, \tilde{n}^* = 0.0633$

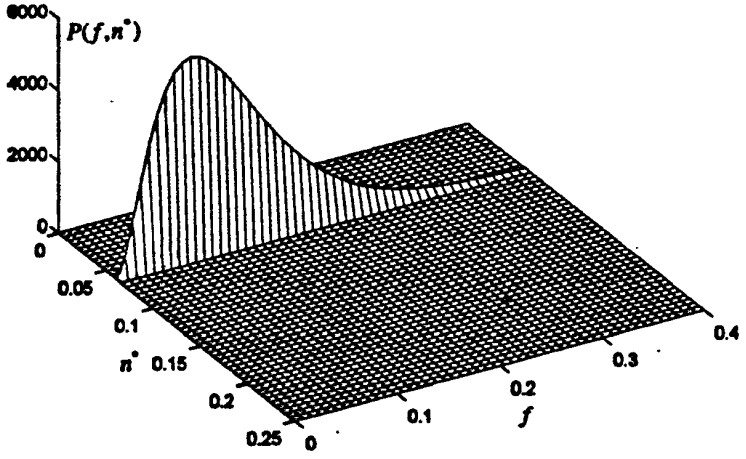

Figure 6(b): Conventional assumed shape pdf $P(f,n^*)$
$\tilde{f} = f_{so}, \tilde{g} = 0.01, \tilde{n}^* = 0.0633$

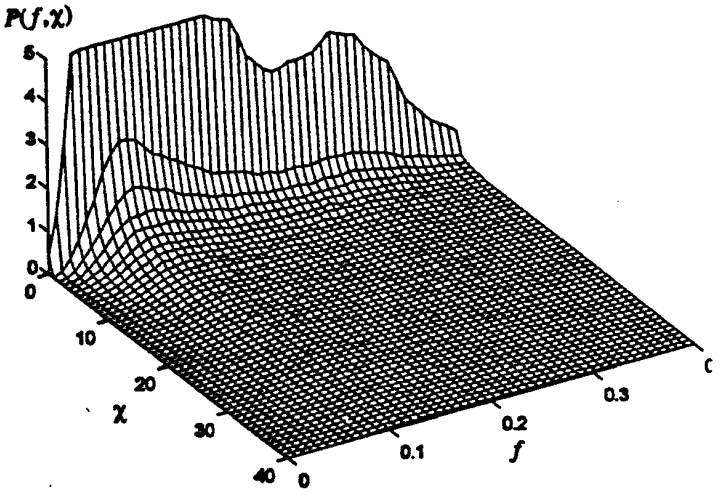

Figure 6(c): LEM pdf $P(f,\chi)$
$\tilde{f} = f_{so}, \tilde{g} = 0.01, \tilde{\chi} = 21.7s^{-1}$

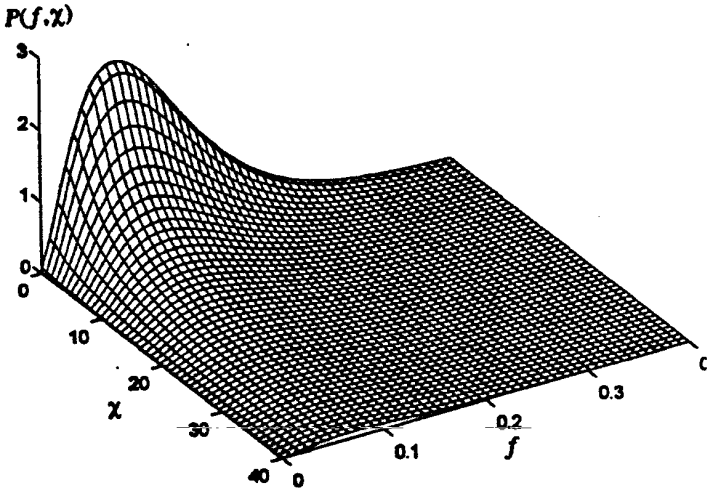

Figure 6(d): Conventional assumed shape pdf $P(f,\chi)$
$\tilde{f} = f_{so}, \tilde{g} = 0.01, \tilde{\chi} = 21.7s^{-1}$

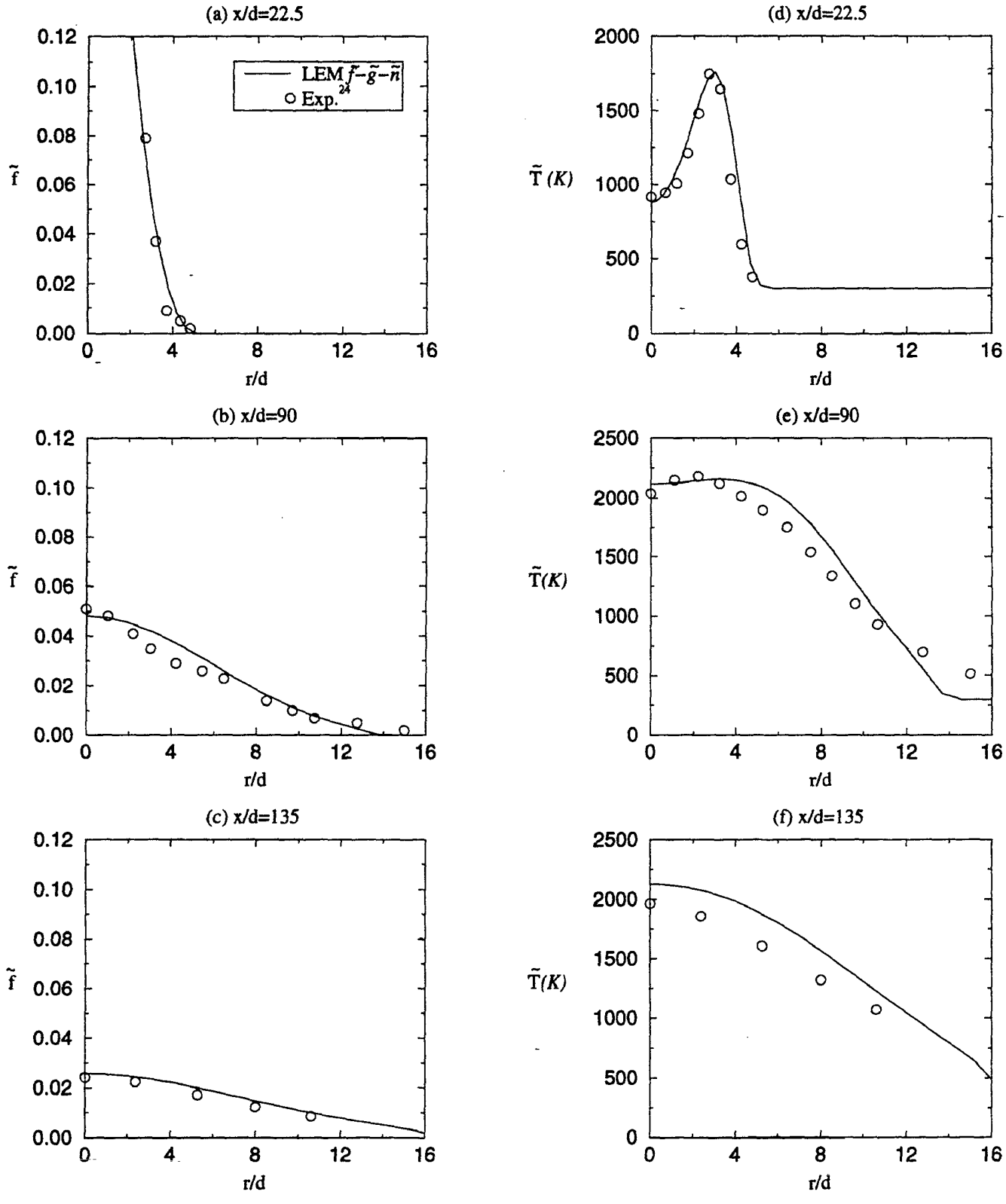

Figure 7
Experimental[24] and predicted $\tilde{f}$ and $\tilde{T}$ in a turbulent H_2 jet flame

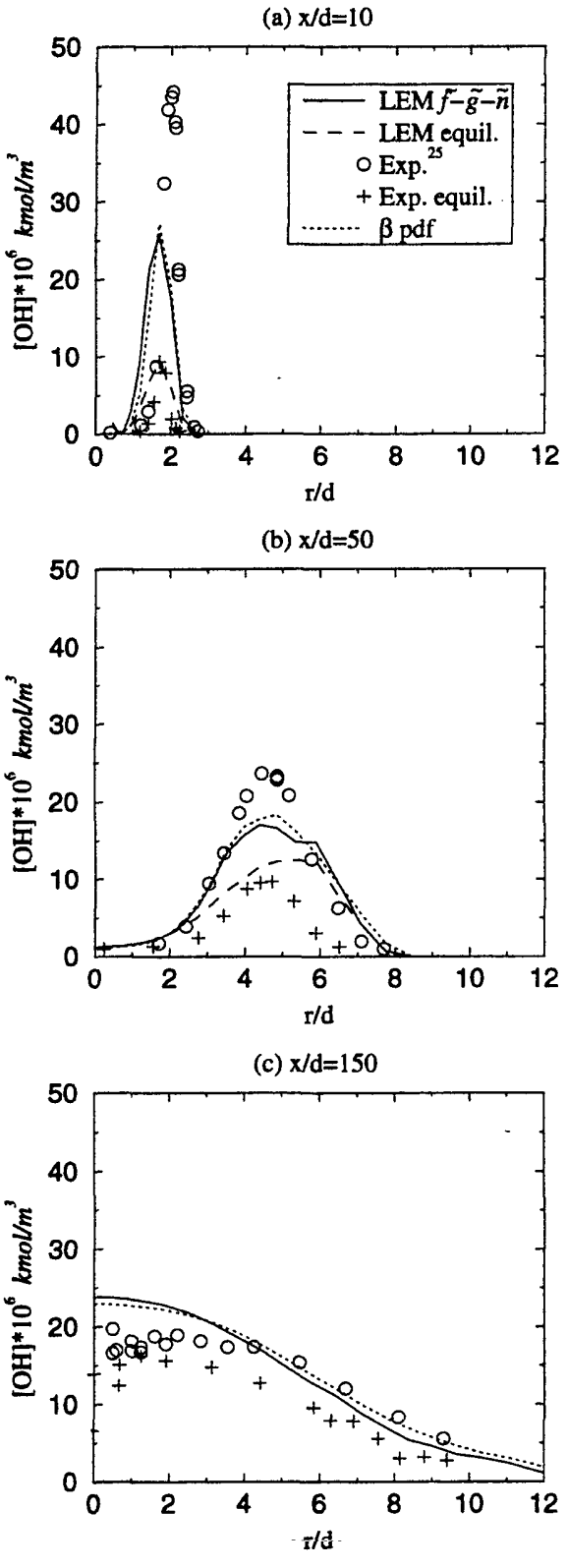

Figure 8
Experimental[25] and predicted (with a $\tilde{f}-\tilde{g}-\tilde{n}$ table) mean *OH* concentration in a turbulent H_2 jet flame

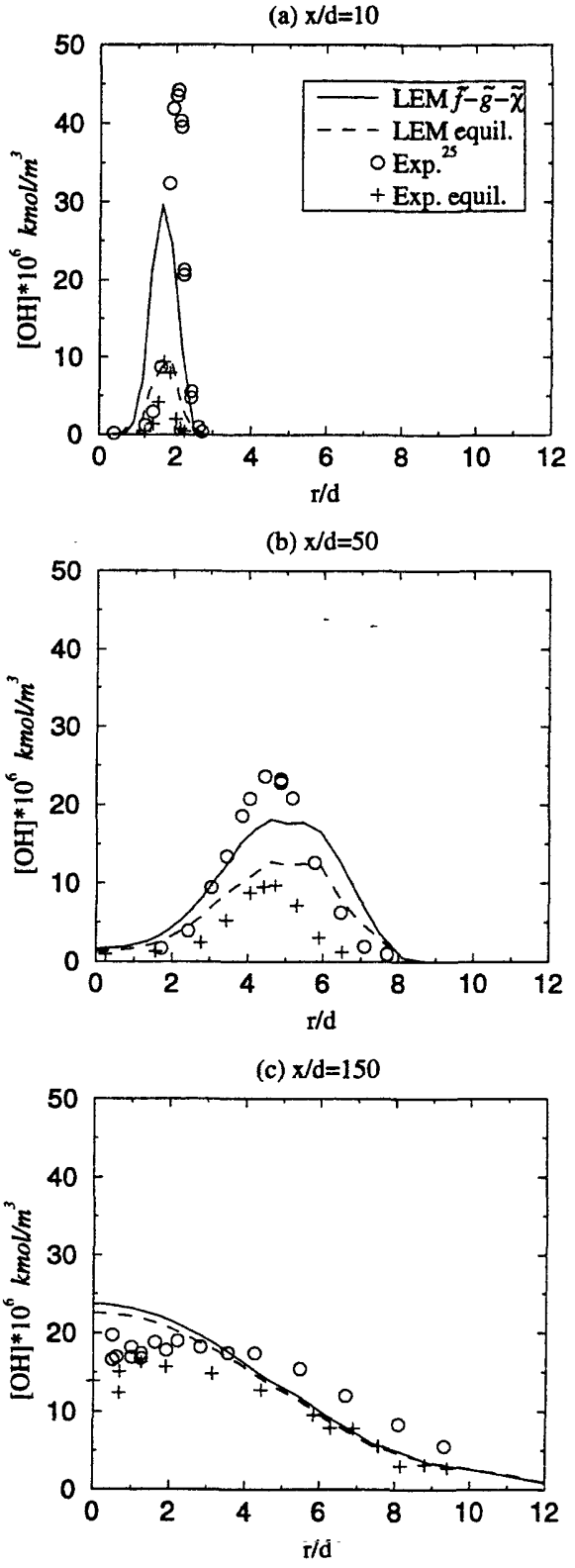

Figure 9
Experimental[25] and predicted (with a $\tilde{f}-\tilde{g}-\tilde{\chi}$ table) mean *OH* concentration in a turbulent H_2 jet flame